Characterization of a Cold Atmospheric Pressure Plasma Jet Device Driven by Nanosecond Voltage Pulses

Characterization of a Cold Atmospheric Pressure Plasma Jet Device Driven by Nanosecond Voltage Pulses

in IEEE Transacitons on Plasma Science,vol. 43, 3, 2015

Characterization of a Cold Atmospheric Pressure Plasma Jet Device Driven by Nanosecond Voltage Pulses

Marco Boselli, Vittorio Colombo, Matteo Gherardi, Romolo Laurita, Anna Liguori, Paolo Sanibondi, Emanuele Simoncelli, and Augusto Stancampiano

***Abstract*— The structure, fluid-dynamic behavior, temperature, and radiation emission of a cold atmospheric pressure plasma jet driven by high-voltage pulses with rise time and duration of a few nanoseconds have been investigated. Intensified charge-coupled device (iCCD) imaging revealed that the discharge starts when voltage values of 5–10 kV are reached on the rising front of the applied voltage pulse; the discharge then propagates downstream the source outlet with a velocity around 10^7–10^8 cm/s. Light emission was observed to increase and decrease periodically and repetitively during discharge propagation. The structure of the plasma plume presents a single front or either several branched subfronts, depending on the operating conditions; merging results of investigations by means of Schlieren and iCCD imaging suggests that branching of the discharge front occurs in spatial regions where the flow is turbulent. By means of optical emission spectroscopy, discharge emission was observed in the ultraviolet-visible (UV-VIS) spectral range (N_2, N_2^+, OH, and NO emission bands); total UV irradiance was lower than 1 μW/cm^2 even at short distances from the device outlet (<15 mm). Plasma plume temperature does not exceed 45 °C for all the tested operating conditions and values close to ambient temperature were measured around 10 mm downstream the source outlet.**

***Index Terms*— Cold atmospheric pressure plasma jets (APPJs), plasma diagnostics, material and biomedical applications.**

I. Introduction

In RECENT years, nonequilibrium atmospheric pressure plasma jets (APPJs) have been raising a significant interest because of their broad range of applications, among which the decontamination and sterilization of surfaces [1], [2], surface modification of polymers [3]–[5], thin film deposition [6], [7], and nanomaterials fabrication and modification [8]–[12]. Moreover, APPJs are widely investigated for plasma-assisted medical therapies: starting with the pioneering works from [13], APPJs have been evaluated for numerous applications at the forefront of research, ranging from blood coagulation and chronic wound remediation to cancer treatment [14]–[27].

One of the reasons of the diffuse interest toward APPJs is their versatility, granted by the diverse possible combinations of driving power supply, gas employed, and source architecture [28]; among this ample number of plasma sources, APPJs notable for their scientific and historical relevance, characteristic architecture, or extensive application are the plasma needle [29], the plasma gun [30], the plasma pencil [31], the kINPen [32], the plasma jet array or *Gatling machine gun-like* plasma jet [33], [34], and the plasma jet with the porous alumina layer between anode and cathode developed in [35].

Several studies have been devoted to the investigation of physical and chemical phenomena taking place in the discharge generated by APPJs [32], [36]–[42]. A particular attention in APPJs characterization has been dedicated to discharge structure since the first works reporting on the observation of plasma bullets [43]–[45], whose fundamental aspects are still debated within the international scientific community; indeed, a new theory was recently introduced along with a new nomenclature (pulsed atmospheric-pressure plasma streams) [46], [47]. An extensive review on the theoretical and experimental studies on plasma bullets has been published earlier this year [48].

In this paper, the characterization of a single electrode (SE) plasma jet driven by voltage pulses with nanosecond rise time and pulse duration in the order of few tens of nanoseconds is presented. The plasma source, developed by the authors, was previously adopted for the treatment of polymer solutions to increase nanoparticle dispersion [49] and to improve the electrospinnability of poly (L-lactic acid) for the production of high quality solvent free nanofibrous scaffolds for biomedical applications [50], [51]; moreover, the plasma jet has been previously investigated in terms of fluid-dynamic behavior and it has been shown that turbulent or laminar regimes can be obtained changing the operating conditions of the plasma source [52]. Here, we present a deeper characterization of the APPJ device, exploiting a set of techniques to get deeper insights on the correlation between the plasma structure and fluid-dynamic behavior of the jet (by means of iCCD and

Manuscript received June 30, 2014; revised October 14, 2014; accepted December 8, 2014. This work was supported in part by European Cooperation in Science and Technology (COST) Action through the Project entitled Biomedical Applications of Atmospheric Pressure Plasma Technology under Grant MP1101, in part by COST Action through the Project entitled Electrical Discharges With Liquids for Future Applications under Grant TD1208, and in part by the Alma Mater Studiorum-Università di Bologna through the University Fundings For Basic Research entitled Plasmat.

The authors are with the Department of Industrial Engineering and Industrial Research Centre for Advanced Mechanics and Materials, Alma Mater Studiorum-Università di Bologna, via Saragozza 8, Bologna 40123, Italy (e-mail: vittorio.colombo@unibo.it).

Color versions of one or more of the figures in this paper are available online at http://ieeexplore.ieee.org.

Digital Object Identifier 10.1109/TPS.2014.2381854

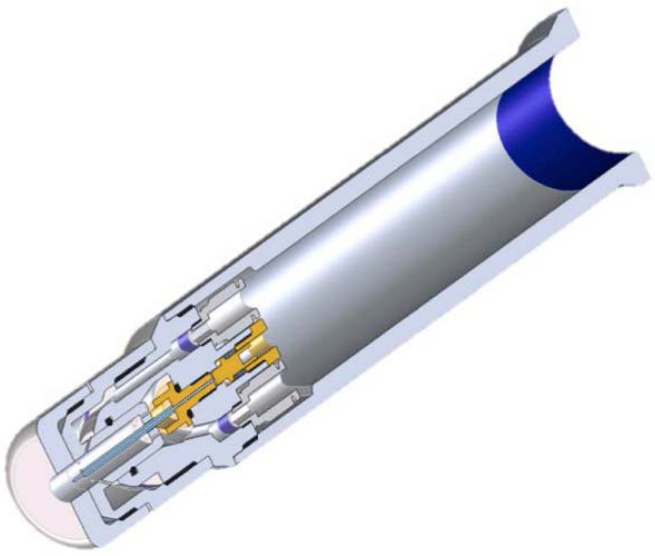

Fig. 1. 3-D cross-sectional representation of the plasma source adopted in the experiments [50].

high-speed Schlieren imaging) and to assess the compatibility of the plasma jet for the treatment of thermosensible materials and for biomedical applications (by means of temperature measurements, optical emission spectroscopy, and UV absolute radiometry).

II. Experimental Setup

A. Cold Atmospheric Pressure Plasma Jet Source

The plasma source adopted in this paper is a SE plasma jet developed in our laboratory and previously reported in [49]–[52]. A schematic of the plasma source is shown in Fig. 1. The high-voltage SE is a 19.5 mm long stainless steel sharpened metallic needle with a diameter of 0.3 mm; the electrode protrudes from a quartz capillary (outer diameter of 1 mm) by 3 mm. In this source, a primary gas [Ar, helium (He), and air] is introduced for sustaining the plasma, whereas a secondary gas (O_2, N_2, gas-phase monomer) can be introduced when required in specific applications. The primary gas is injected through a 12-hole (0.3 mm diameter) diffuser aimed at ensuring a uniform and laminar flow along the electrode and at sustaining the plasma discharge, while the secondary gas is introduced in the discharge region downstream the electrode tip through twelve 0.3 mm holes, tilted with respect to the plasma source axis. The plasma is ejected through a 1 mm orifice [50], [52]. In this paper, the primary gas used is He, whereas no secondary gas was employed.

The plasma source is driven by a commercial pulse generator (FID GmbH—FPG 20–1NMK) producing high-voltage pulses with a slew rate of few kilovoltages per nanosecond, a pulse duration around 30 ns, a peak voltage (PV) of 7–20 kV, and an energy per pulse of 50 mJ at maximum voltage amplitude into a 100–200 Ω load impedance with a maximum pulse repetition frequency (PRF) of 1000 Hz.

B. iCCD Imaging

Temporal evolution of the plasma discharge has been investigated by means of an iCCD camera (Princeton Instruments PIMAX3). A pulse generator (BNC 575 digital pulse/delay generator) has been used to synchronize the generator, the oscilloscope (Tektronix DPO 40034), and the iCCD camera. Two configurations of the iCCD camera have been adopted: in the first configuration, several sequential frames at time steps of 0.25 ns and with an exposure time of 3 ns [50 accumulations collected on the charge coupled device (CCD) sensor for each frame] have been acquired to track the temporal evolution of the plasma discharge during the high-voltage pulse; in the second configuration, a single frame with exposure time of 35 ns covering the entire voltage pulse has been acquired with the aim of comparing the discharge structure and the fluid-dynamic behavior of the jet, which has been observed through Schlieren imaging.

C. Schlieren Imaging

A Schlieren imaging setup in a Z-configuration [52] has been adopted to visualize refractive-index gradients generated in the region downstream the plasma source outlet by the plasma gas mixing with the surrounding ambient air. The imaging setup is composed of a 450 W ozone free xenon lamp (Newport-Oriel 66355 Simplicity Arc Source), a slit and an iris diaphragm, two parabolic mirrors with a focal length of 1 m, a knife edge positioned vertically, and a high-speed camera (Memrecam K3R-NAC Image Technology, operated at 4000 frames/s and 1/50 000-s shutter time) that records the Schlieren image. The plasma jet has been positioned in the middle of the optical path between the two parabolic mirrors, as shown in Fig. 2.

D. Temperature Measurements

Plasma jet temperature has been measured by means of a fiber optic temperature sensor (OPSENS OTP-M) with a calibration range of 20 °C–60 °C, a resolution of 0.01 °C, an accuracy of 0.15 °C, and a response time of less than 1 s.

The fiber optic sensor head has a cylindrical shape with a radius of 1.2 mm and a length of 7 mm. During measurement, the sensor head was positioned coaxially with the source orifice. A second fiber optic sensor was employed to monitor the room temperature during the measurements. Fiber optic sensors have been chosen for measurements because they are immune from electromagnetic interferences [53] and they only slightly affect the discharge because of the small diameter and the dielectric properties of the sensor head.

E. Optical Emission Spectroscopy

An iCCD camera (PIMAX3, Princeton Instruments) mounted on a 500 mm spectrometer (Acton SP2500i, Princeton Instruments) has been adopted to collect spatially resolved optical emission spectra in the UV, VIS and near infrared (NIR) regions. Details of the experimental setup can be found in [50]. Measurements have been performed using a lens with 30 mm focal length and a 20 μm slit width to collect spectra in the region extending from the source outlet to 15 mm downstream, with a spatial resolution of 0.1 mm and a spectral resolution of 0.17 nm. Exposure time has been set at 20 μs and for each spectrum a set of 50 accumulations has been collected on the CCD sensor.

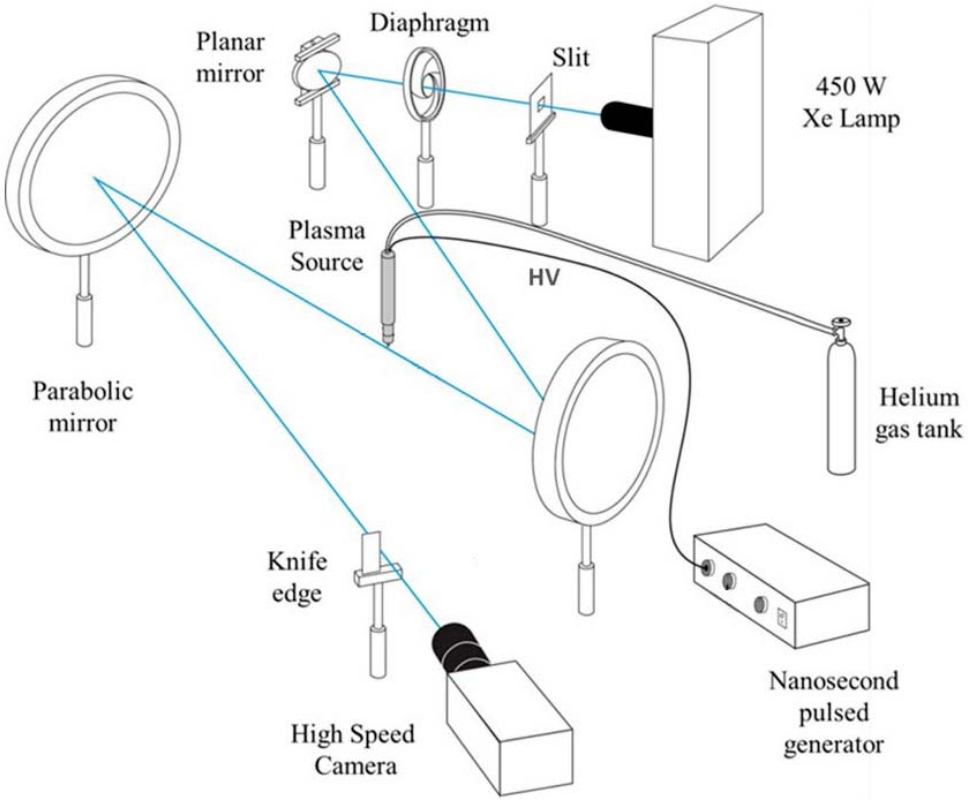

Fig. 2. Experimental setup for high-speed Schlieren imaging of the plasma jet.

F. UV Irradiance Measurement

UV irradiance has been measured using the UV power meter Hamamatsu C9536/H9535-222 (measurement range of 0.001–200 mW/cm^2, high spectral response in the range 150–350 nm). The sensor head, covered with a quartz disk to avoid direct exposure to the plasma jet, has been positioned downstream the plasma source outlet. The protecting quartz disk (thickness = 0.5 mm and diameter = 35 mm) is characterized by an integral UV transmission of 93% across the sensor spectral range. The sensitive part of the UV power meter was centered on the axis of the source orifice so that the plasma plume was directly impinging on the protective quartz disk. Measurements have been carried out at different axial distances from the source outlet.

III. Results

A. Structure of the Plasma Discharge

The structure of the plasma jet and its evolution in time have been investigated for two different sets of operating conditions, inducing strongly different plasma characteristics: in the first case, PV, PRF, and mass flow rate were set to 17 kV, 1000 Hz and 2 SLPM of He respectively; in the second case, the PV and mass flow rate were increased to 25 kV and 3 SLPM of He, respectively.

The iCCD camera has been set to scan the voltage pulse with an exposure time of 3 ns. The iCCD gate opening for the first recorded frame of each scan was set at the start of the voltage pulse and subsequent frames were recorded at fixed time steps of 0.25 ns; therefore, two consecutive frames overlap for 2.75 ns.

For the first case, a sequence of representative frames is shown in Fig. 3, where the time values reported on top of each frame are indicative of the time lapse between the start of the voltage pulse and the corresponding opening of the iCCD gate. For the sake of clarity, the exposures of the most relevant frames depicted in Fig. 3 are reported, together with the high-voltage pulse waveform, in Fig. 4.

The plasma plume appears 5 ns after the start of the voltage rise, which corresponds to a voltage in the range 5–10 kV, and it can be observed in all the subsequent frames taken during the voltage pulse. Nevertheless, its intensity and extension seem to fluctuate during the high-voltage pulse. For example, from the frame starting at 5 to the one at 9.75 ns, both the intensity and the length of the plasma plume increase up to a maximum reached at 6.75 ns and then they start to decrease. A similar behavior can be observed every 5 ns: from 10 to 15 ns, from 15 to 20 ns, and from 20 to 25 ns. To the best of the authors' knowledge, this fluctuating behavior has never been reported in the literature before.

Considering only the brightest frame in each fluctuation (6.75, 11.75, 16.75, and 21.75 ns), a progressive elongation of the plasma plume is clearly visible. As it can be observed in the frames reported in Fig. 3 with a chromatic scale modified to enhance the light emissions with lower intensity, the propagating plasma front remains connected to the plasma source by a VIS channel even in the frames in which the plasma plume is characterized by weaker intensity. This structure,

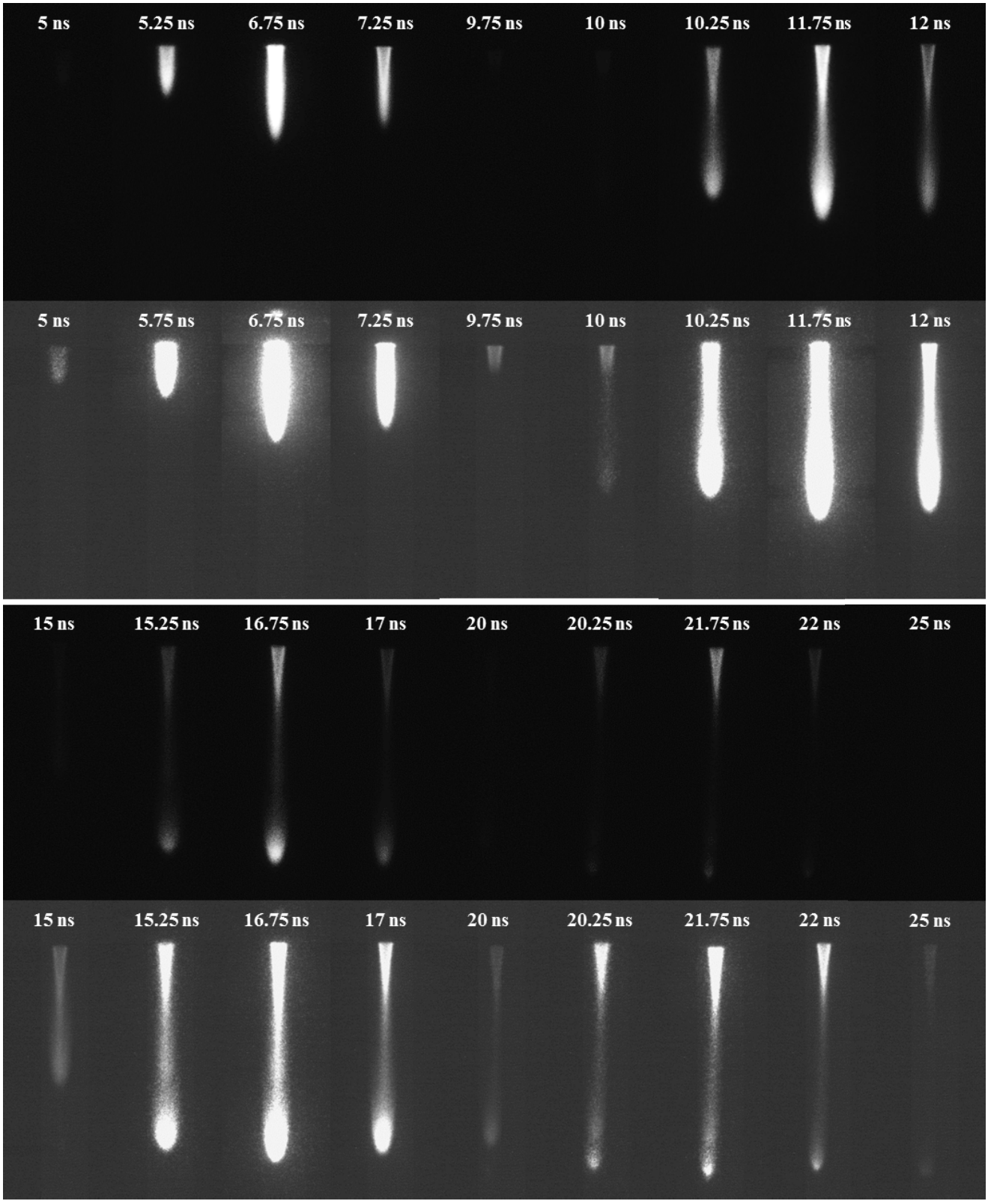

Fig. 3. iCCD frames (3 ns exposure time, 50 accumulations) for the case with 17 kV (PV), 1000 Hz (PRF), and 2 SLPM of He as working gas. Two different chromatic scales were adopted to make all the frames clearly visible (top—higher intensity scale and bottom—low intensity scale). The time values reported on top of each frame are indicative of the time lapse between the start of the voltage pulse and the corresponding opening of the iCCD gate.

characterized by a moving front connected to the source, is similar to what already reported in the literature for other plasma jet sources [54]–[56].

By tracking the temporal evolution of the plasma plume, it is possible to estimate the velocity of the front propagation. The obtained values are in the order of 10^8 cm/s during the

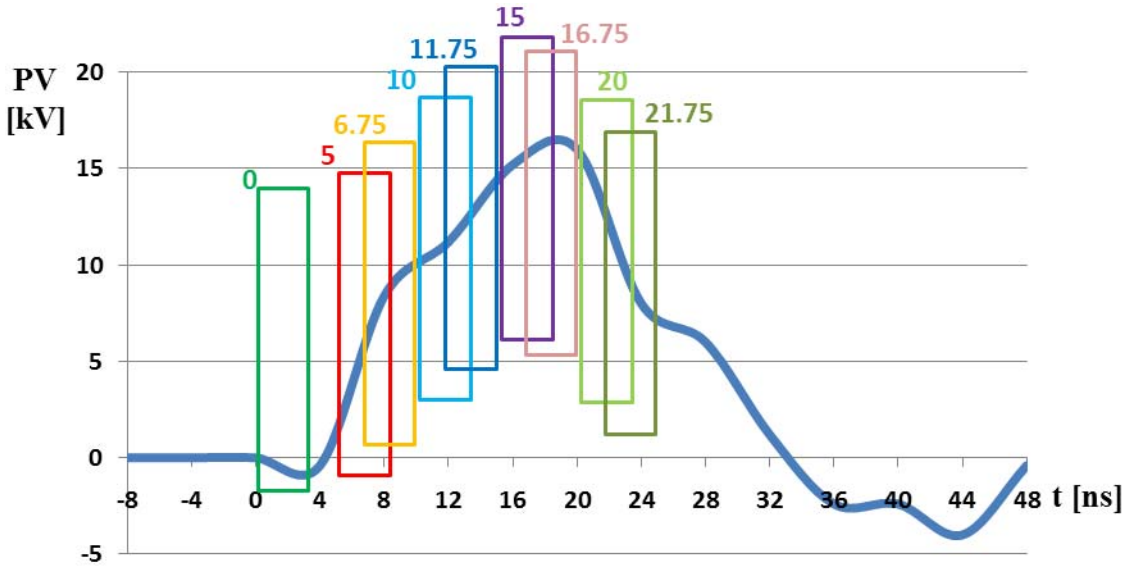

Fig. 4. Voltage waveform for the case with 17 kV (PV), 1000 Hz (PRF), and 2 SLPM of He as working gas with superimposed exposures for relevant iCCD frames. The time values reported on top of each exposure are indicative of the time lapse between the start of the voltage pulse and the corresponding opening of the iCCD gate.

first acquired frames (from 5 to 7.25 ns) and the velocity is reduced to 5×10^7 cm/s when the PV is reached. Similar values have been reported for other plasma jet sources driven by voltage pulses with nanosecond rise time [30], [57], [58].

A similar analysis has been conducted for the second case and results are reported in Figs. 5 and 6. In this case too, it is possible to observe a fluctuation of both the intensity and the length of the plasma plume with a period (5 ns) similar to that observed in the first case. Nevertheless, the structure of the plasma evolves in a sensibly different way. While in the first case, only one front can be observed in the plasma jet, in the second case, the final part of the plasma jet is at first distorted (frames at 11 and 11.25 ns in Fig. 5) and then branched in several fronts connected to the plasma source by converging tails characterized by weaker emission (frames at 16 and 16.25 ns).

A behavior of the plasma front similar to the one observed at instants 11 and 11.25 ns has been observed in [59] and described as snake-like mode. This aspect, as well as the subsequent branching of the plasma jet front, is probably related to hydrodynamic instabilities of the He gas flow, which result in turbulent mixing of He species with the surrounding ambient air; as the plasma discharge is propagating preferentially in regions with high He concentration [60], the turbulent mixing of He and surrounding air can induce several pathways for the plasma discharge, resulting in branching of the plasma jet front. To investigate the correlation between the gas flow instabilities and discharge structure, further investigations exploiting Schlieren imaging have been conducted and the results are presented in the following paragraph.

B. Influence of Jet's Fluid Dynamics on Discharge Structure

Schlieren high-speed recordings of the fluid-dynamic behavior of the plasma jet and iCCD images of the discharge structure have been acquired for the different operating conditions of the plasma source. The He flow rate has been kept fixed at 3 SLPM while the PV and the PRF have been changed in the range 17–30 kV and 125–1000 Hz, respectively.

Since the duration of the high-voltage pulse driving the plasma source is less than the time span of each Schlieren high-speed camera frame (0.25 ms at 4000 frames/s), the fluid-dynamic phenomena occurring during the voltage pulse are observed in a single frame. This frame has been reported in Fig. 7 for different operating conditions of the plasma source together with the corresponding iCCD acquisition performed with an exposure window of 35 ns to collect light emitted during the whole high-voltage pulse.

From Schlieren images, it can be noted that the flow at the source outlet is almost laminar (Reynolds number is approximately 500 for the plasma source operated with 3 SLPM of He) while fluid-dynamic instabilities can be observed in a more downstream position. With increasing PRF (from 125 to 1000 Hz), the length of the laminar region becomes shorter and fluid-dynamic instabilities of higher intensity can be observed. With PV increasing from 17 to 30 kV, the same trend is observed, but the effect is weaker in comparison with the change in PRF.

From iCCD images, it can be noted that the length of the plasma plume is increased as the PV is increased, whereas with increasing PRF, the plasma plume length is generally reduced.

From the comparison of Schlieren frames and iCCD images, a clear correspondence between fluid-dynamic instabilities and branching of the plasma plume can be observed. The ending part of the plasma plume becomes branched in the cases in which the operating conditions induce the plasma plume to propagate into the spatial region where the flow is turbulent. This phenomenon is mostly evident for the cases with highest PV (30 kV), which are characterized by a longer plasma plume that can penetrate the regions with higher intensity of fluid-dynamics instabilities. It should be noted that the branching of the plasma plume appears in correspondence of the region where the transition from laminar to turbulent flow is observed.

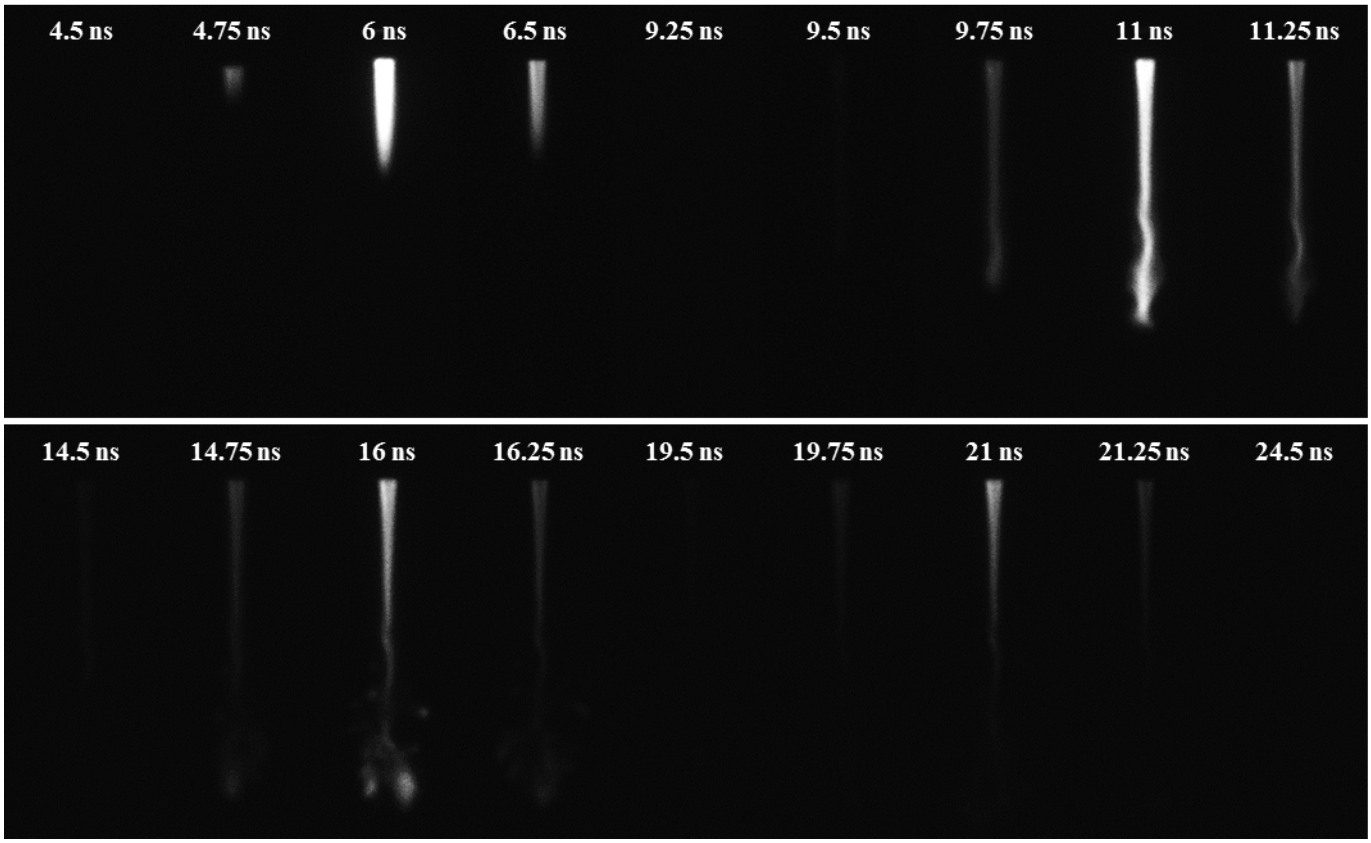

Fig. 5. iCCD frames (3 ns exposure time, 50 accumulations) for the case with 25 kV (PV), 1000 Hz (PRF), and 3 SLPM of He as working gas. The time values reported on top of each frame are indicative of the time lapse between the start of the voltage pulse and the corresponding opening of the iCCD gate.

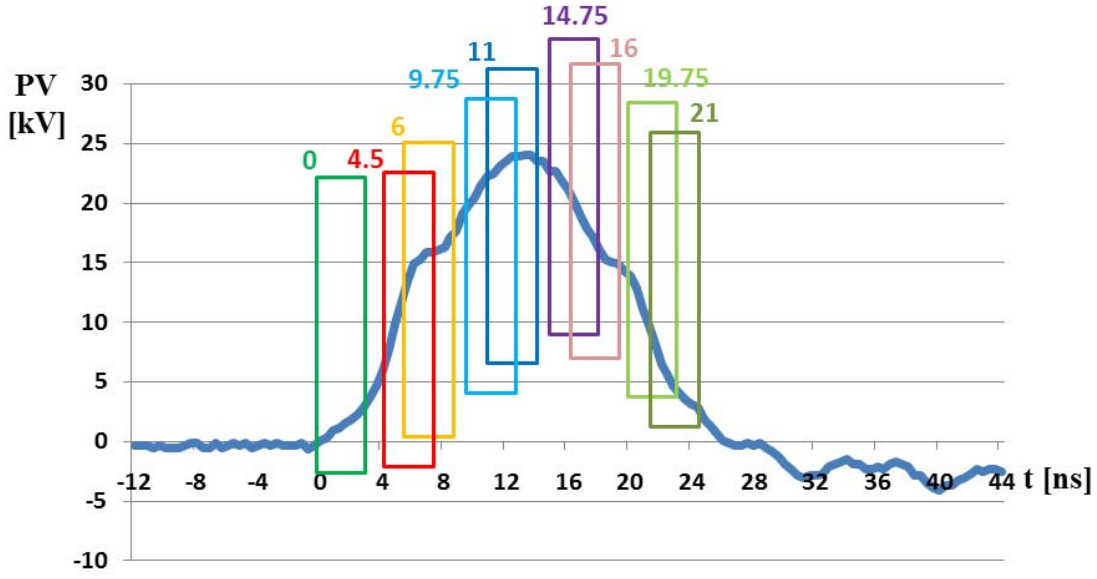

Fig. 6. Voltage waveform for the case with 25 kV (PV), 1000 Hz (PRF), and 3 SLPM of He as working gas with superimposed exposures for relevant iCCD frames. The time values reported on top of each exposure are indicative of the time lapse between the start of the voltage pulse and the corresponding opening of the iCCD gate.

On the contrary, in the cases with lowest PV (17 kV), the plasma plume is propagating in the laminar region only and no branching of the front is observed.

These results support the idea that fluid-dynamic instabilities of the jet induce a turbulent mixing of He and the surrounding air and, consequently, the formation of more than one preferential pathways through which the plasma plume can propagate, resulting in branching of the plasma front.

C. Gas Temperature in the Plasma Jet

Plasma jet temperature has been measured during operation with a PRF varying between 125 and 1000 Hz, PV in the range 17–25 kV, and He flow rate at 1 or 3 SLPM.

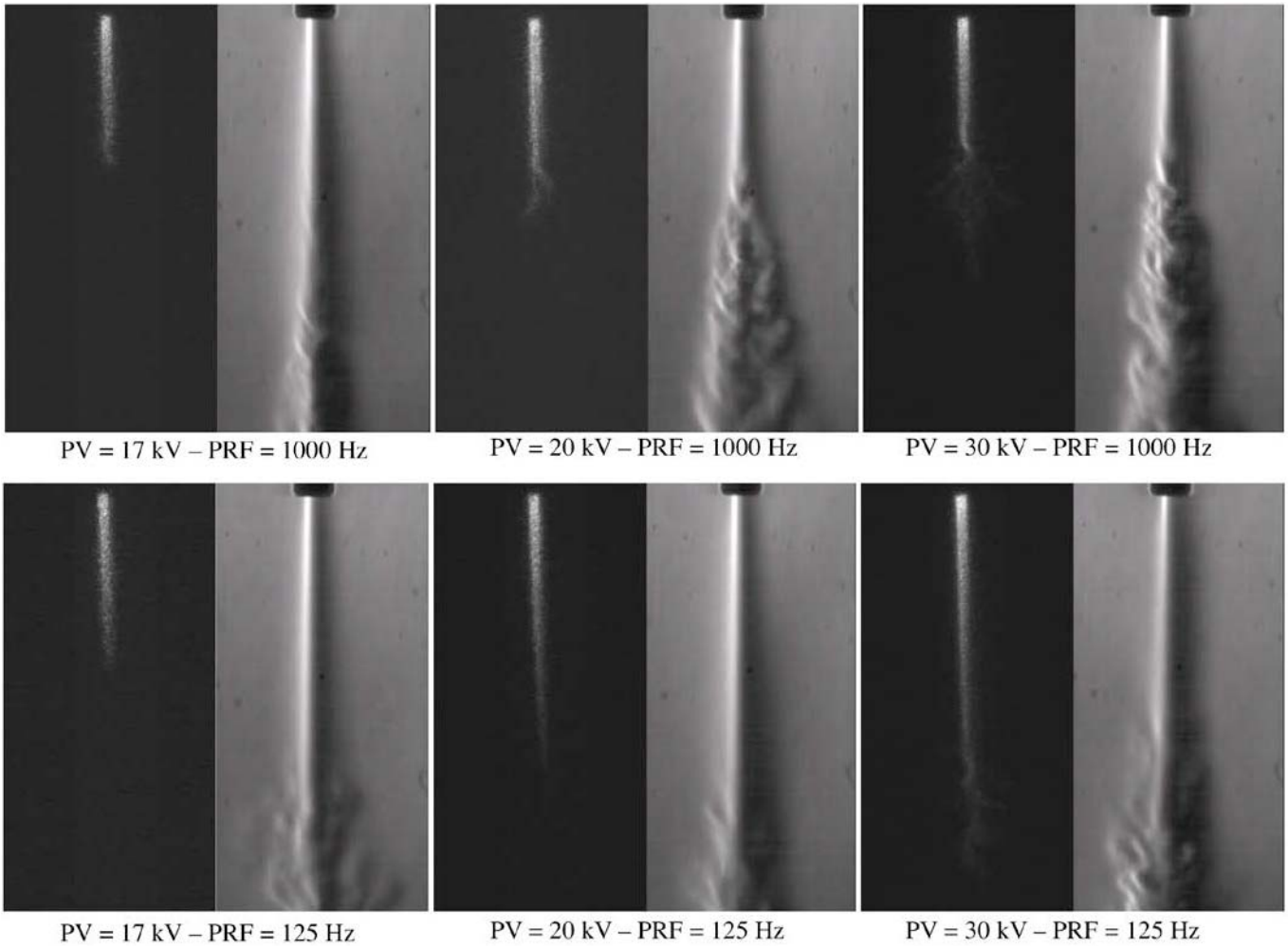

Fig. 7. Comparison of synchronized (left) iCCD and (right) Schlieren acquisitions of the plasma jet for different values of PV (17, 20, and 30 kV) and PRF (125 and 1000 Hz). Flow rate set at 3 SLPM of He for all cases.

Axial temperature profiles (with the axial position defined as the distance measured from the sensor tip to the source outlet; so axial position = 0 mm corresponds to the source outlet) are presented for four different operative conditions with a fixed PRF of 125 and 1000 Hz in Figs. 8 and 9, respectively. Three different measurements have been carried out for each operating condition.

It should be noted that in all the investigated cases, the maximum gas temperature measured by means of fiber optic sensor in the region downstream the source outlet is lower than 45 °C.

For the cases with PRF = 125 Hz (Fig. 8), the temperature is lower than 40 °C. In particular, in the cases with a flow rate of 1 SLPM, the maximum temperature is reached in the region close to the source outlet and a steep decrease of the temperature is observed at 6 and 12 mm downstream plasma source tip for the cases with PV at 17 and 25 kV, respectively. With a higher flow rate (3 SLPM of He), the temperature profile is almost uniform along the axis and the peak value is close to room temperature.

An increase of PRF up to 1000 Hz, as shown in Fig. 9, induces an increase of the plasma temperature in the zone closest to the plasma tip, reaching a maximum temperature of 45 °C for the case with highest peak voltage and lowest flow rate. For the case with 1 SLPM of He, when the plasma is driven by a PV of 25 kV, a drastic drop of temperature is observed 10 mm downstream the plasma source, while a smoother decrease is observed for lower applied voltage. For a higher flow rate (3 SLPM of He), a flatter temperature profile is registered with respect to the cases with flow rate at 1 SLPM of He) with values close to the ambient temperature.

D. Optical Emission Spectroscopy and UV Irradiance Measurements

Optical emission spectra in the UV–VIS–NIR regions as a function of both the wavelength and the distance from the source outlet are shown in Fig. 10 for the plasma jet operated with a PV of 20 kV, a PRF of 125 Hz, and a He gas flow rate of 3 SLPM.

Optical radiation is emitted mainly in the UV-VIS region, where bands of excited molecular nitrogen (second positive system of N_2) can be found between 280 and 450 nm, together with OH radicals in the Ultraviolet B region at 307 nm. Emission from the first negative system of N_2^+ is detected

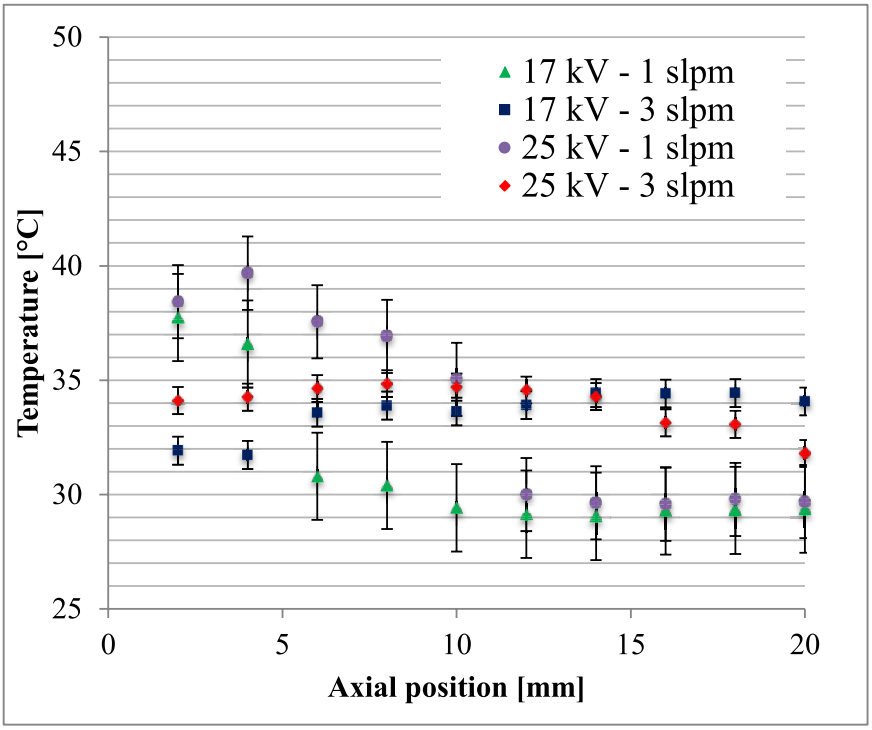

Fig. 8. Axial temperature profile of the plasma jet at constant PRF (125 Hz) for different values of PV (17 and 25 kV) and He flow rate (1 and 3 SLPM). Room temperature during measurements around 29 °C. Axial position = 0 mm corresponds to the source outlet.

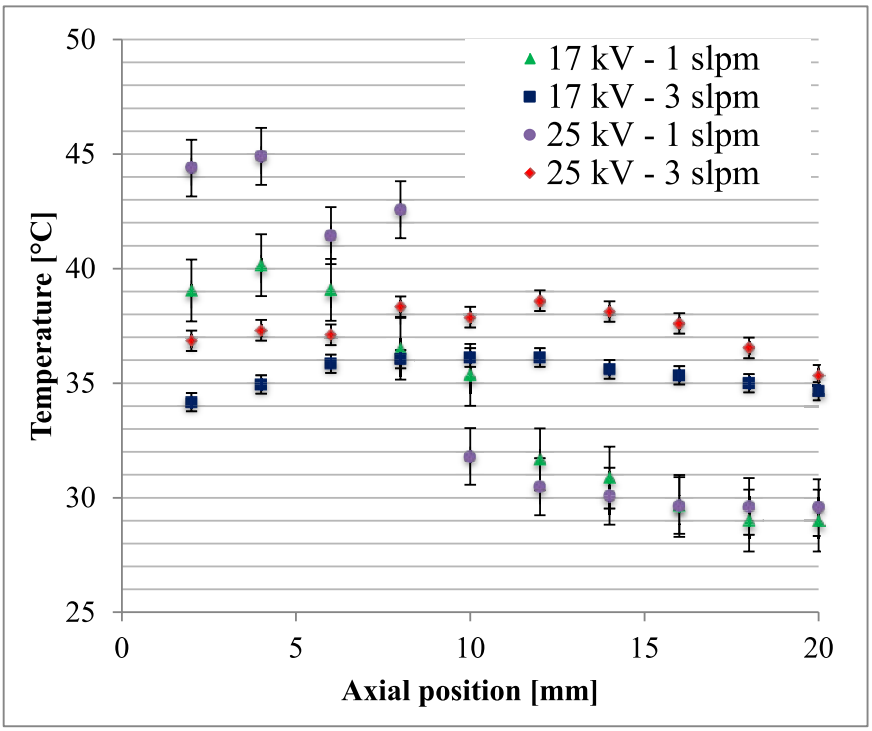

Fig. 9. Axial temperature profile of the plasma jet at constant PRF (1 kHz) for different values of PV (17 and 25 kV) and He flow rate (1 and 3 SLPM). Room temperature during measurements: around 29 °C. Axial position = 0 mm corresponds to the source outlet.

at 391, 427, and 470 nm. A faint emission in the UVC region between 250 and 280 nm due to NO radicals was also observed.

In VIS-NIR, only a few lines of He and O and the second-order diffractions of N_2 and N_2^+ systems can be observed. He lines were registered at 501, 587, 667, and 706 nm. Emission of atomic oxygen was observed at 777 nm. Spectral bands observed between 675 and 760 nm are generated by second-order diffractions of the monochromator and are related to N_2 emission bands.

As the plasma gas is He, at the axial position corresponding to the outlet of the plasma source, only the emission from He lines is observed. At higher distance from the source outlet, the surrounding air is diffusing into the plasma gas and the

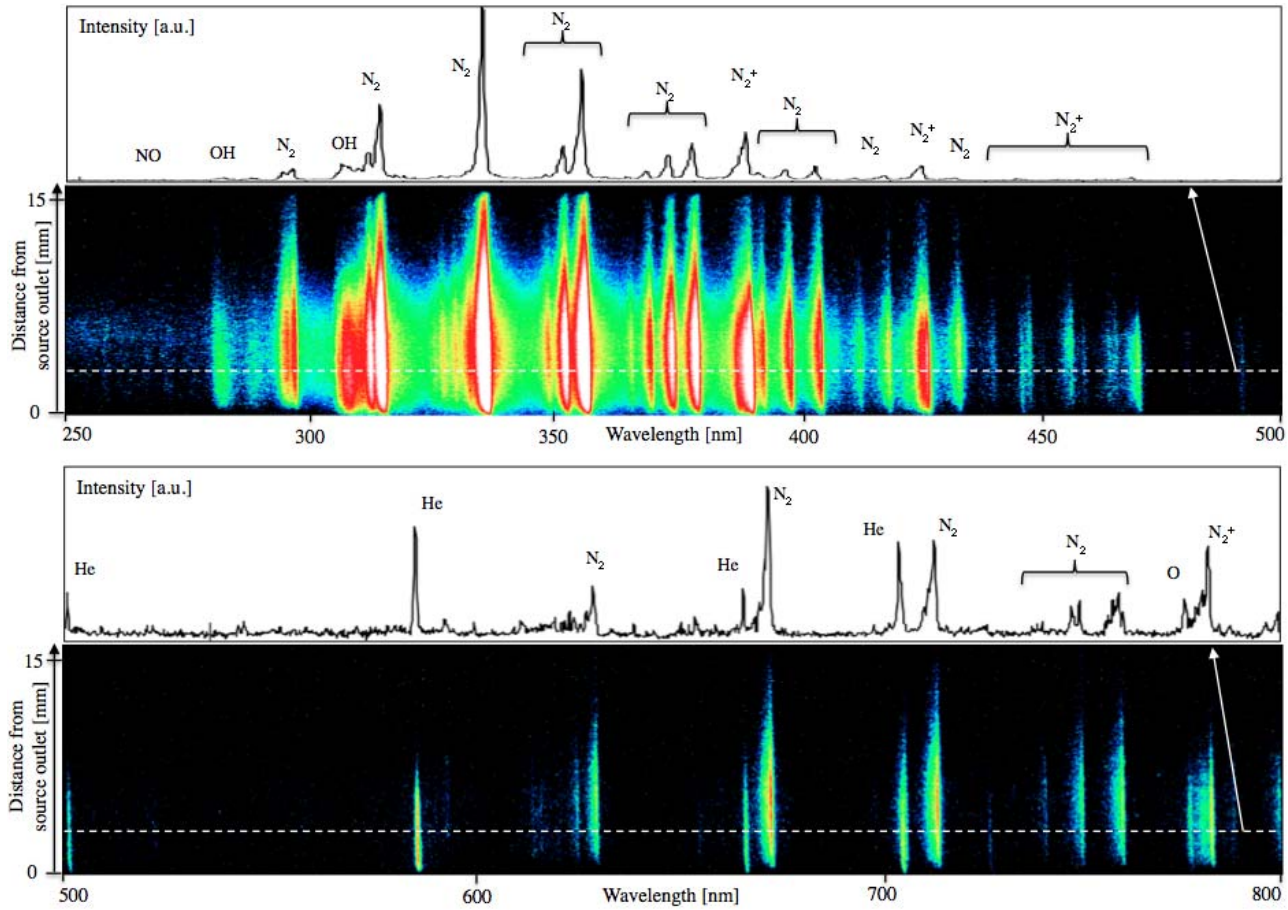

Fig. 10. Optical emission spectra in (top) UV-VIS and (bottom) VIS-NIR range as a function of both the wavelength and the distance from the source outlet. Plasma jet operated with PV = 20 kV, PRF = 125 Hz, and He flow rate = 3 SLPM.

emission bands of excited N_2, OH, and NO can be observed, which are characterized by maximum intensity positioned approximately at 6 mm downstream the source outlet. This can be explained as the emission intensity of these bands depends on: 1) the concentration of ground state molecules and 2) the rate of molecule excitation; while the concentration of ground state molecules increases the further from the source outlet, as a consequence of an increasing mole fraction of air due to diffusion into the plasma gas, the rate of molecule excitation decreases the further from the outlet, because of the decrease of the local electric field intensity (being the plasma source of the SE type with a virtual grounded electrode) and because the electron concentration decreases as a consequence of the increasing mole fraction of air. The opposite trends expected for these two parameters can be appointed as responsible for the maximum emission intensity to be at a certain distance from source outlet, which we experimentally determined to be 6 mm, for the considered operating conditions. Similar considerations and results have been previously presented in a computational analysis of a He/O_2 plasma jet flowed into humid air [61].

A qualitatively similar emission spectrum can be observed also for other investigated operating conditions.

The intensity of emission increases for higher values of PV and He gas flow rate, as shown in Fig. 11, where the relative intensities of selected emission bands of OH, N_2, N_2^+, and emission lines of O and He are reported.

The effect of PV increase can be explained in terms of the higher local electric field produced in the plasma plume which, in turn, produces a higher electron concentration that enhances the production of excited species and radiation emission.

Meanwhile, increasing He flow rate (for operating conditions that results in an almost laminar flow in the emitting region, as shown in Fig. 7) was previously shown to result in a lower mole fraction of ambient air in the plasma plume region [48], [62], that can lead to higher local electron concentration [61], which can explain the observed higher emission intensity from excited species.

The effect of He flow rate on the emission intensities from He lines and N_2 bands is further highlighted in Fig. 12. An increase of He flow rate is there shown to result in a higher emission intensity from He species, which extends over a longer region downstream the plasma jet orifice (significant values of emission intensity are measured up to 5 mm downstream for the 1 SLPM case and up to 10 mm for the 3 SLPM case); this enhanced emission intensity can be related to the lower diffusion of air in the plasma region that allows for an increase of electron concentration, He mole fraction in the plume region and, as a consequence, of excited He atoms. A higher He flow rate is also shown to cause

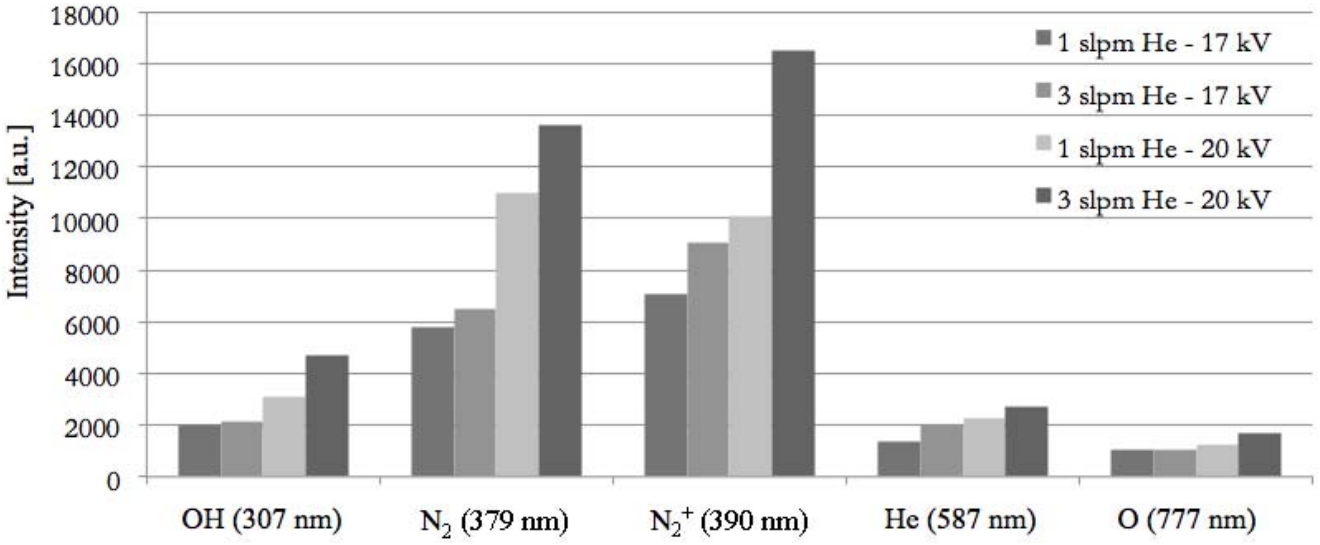

Fig. 11. Relative emission intensity of selected spectral atomic lines and molecular bands for the plasma jet operated with PRF = 125 Hz for different values of PV (17 and 20 kV) and He flow rate (1 and 3 SLPM). For each emission line and band, the value corresponding to the maximum intensity has been reported.

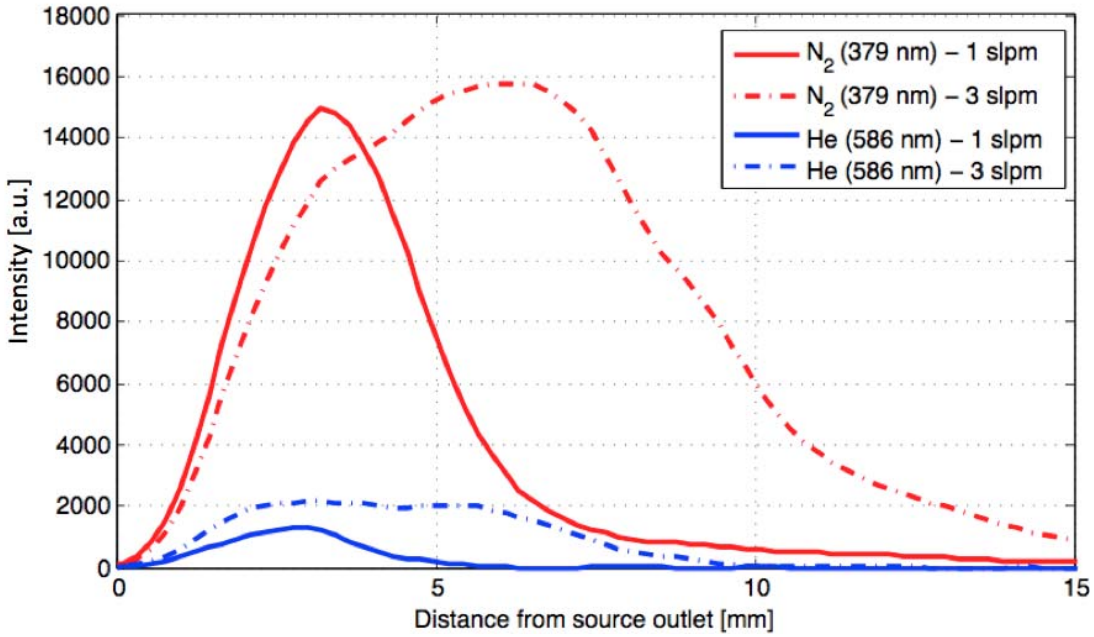

Fig. 12. Relative emission intensity of N_2 molecular band at 379 nm and He atomic line at 586 nm as a function of distance from the plasma source outlet for PRF = 125 Hz, PV = 20 kV, and He flow rate (1 and 3 SLPM).

a higher N_2 peak emission intensity and a significant N_2 emission is observed much further from the source outlet; this can be appointed again to the lower diffusion of air in the plasma region, which results in an increase of electron concentration and, thus, of the N_2 excitation rate. Moreover, the peak of N_2 emission intensity was found to be located further away from the torch outlet in the case with 3 SLPM; indeed, while the higher He flow rate reduces air diffusion in the plasma region and allows for higher electron concentration, it also reduces the mole fraction of ground state N_2 available for excitation in the plasma at a fixed axial position. Therefore, at the same distance from the source outlet where the peak emission intensity was located for the case with 1 SLPM of He (distance of 3 mm), a higher electron concentration and a lower mole fraction of ground state N_2 molecules are expected for the case of 3 SLPM of He, which results in a lower emission intensity. For the latter case, the N_2 peak emission intensity is observed further downstream (distance of 6 mm), where the diffusion of air in the plasma region has enabled the buildup of ground state N_2 mole molecules to be excited, but still has not excessively dampened the electron concentration; at this same axial position, a much lower N_2 emission intensity is observed for the case with 1 SLPM of He, as the higher diffusion of air results in a higher air mole fraction and a faster decrease of electron concentration.

The influence of different operating parameters on the total irradiance in the UV range of the plasma plume has been indirectly evaluated measuring the distance at which an

TABLE I
UV IRRADIANCE MEASUREMENTS FOR DIFFERENT PLASMA JET OPERATING CONDITIONS

Plasma gas flow rate	Pulse repetition frequency	Peak voltage	Distance from source outlet at which UV irradiance = 1 μW/cm^2
1 slpm He	83 Hz	17 kV	<3 mm
1 slpm He	83 Hz	20 kV	<3 mm
3 slpm He	83 Hz	17 kV	<3 mm
3 slpm He	83 Hz	20 kV	9 mm
3 slpm He	125 Hz	17 kV	7.5 mm
3 slpm He	125 Hz	20 kV	12 mm
3 slpm He	1000 Hz	20 kV	15 mm

irradiance of 1 μW/cm^2 can be detected using a UV power meter: the higher is the distance at which UV irradiance = 1 μW/cm^2, the higher is the plasma total UV irradiance. Several plasma operating conditions were tested adjusting He mass flow rate, PV, and PRF.

Results reported in Table I highlight that the plasma UV irradiance increases for higher values of PV, PRF, and gas flow rate.

For a mass flow rate of 1 SLPM of He and low values of both PRF (83 Hz) and PV (17 kV), a UV irradiance of 1 μW/cm^2 can be detected only at a distance of less than 3 mm. Independently increasing the flow rate to 3 SLPM of He, or the PV to 20 kV, no relevant change in UV irradiance can be noticed. By increasing both parameters at the same time, irradiance of 1 μW/cm^2 is reached already 9 mm downstream the source outlet. With flow rate fixed at 3 SLPM of He, increasing the PRF from 83 to 125 Hz results in a higher UV emission (UV irradiance of 1 μW/cm^2 reached at 7.5 and 12 mm for PV set at 17 and 20 kV, respectively).

For the highest flow rate, PV and PRF considered (3 SLPM of He, 20 kV, and 1000 Hz, respectively), the irradiance of 1 μW/cm^2 has been obtained for a distance of 15 mm.

A similar analysis of UV radiation has been carried out by different groups for other plasma sources usually adopted for biomedical applications [32], [63]–[65], with the aim of selecting operating conditions that result in UV irradiances compatible with biomedical treatments. The values obtained for our plasma jet are below those reported in the literature for these plasma sources, which range between 10 and 1000 μW/cm^2.

IV. CONCLUSION

The discharge generated by an APPJ developed by the authors and driven by high-voltage pulses with rise time and duration of a few nanoseconds has been investigated. The plasma plume is characterized by a front propagating with a velocity close to the values reported for plasma bullets (10^7-10^8 cm/s) [30], [57], [58]. The plume presents a single front or several branched subfronts depending on the operating conditions. The comparison of results from Schlieren and iCCD imaging suggests that branching of the plasma jet front occurs in spatial regions where the flow is turbulent. A possible explanation of plume branching is that turbulent mixing of plasma gas and ambient air creates several randomly changing preferential paths characterized by high concentration of He through which the discharge front tends to propagate. It was also observed that the temporal evolution of the plasma plume during the discharge presents oscillations both in light emission intensity and plume length. This phenomenon needs to be further investigated by future studies.

It has been shown that, for a discharge generated in He, the plasma plume is mainly emitting in the UV-VIS range with a spectrum characterized by N_2, N_2^+, NO, and OH spectral bands as a consequence of mixing with ambient air. The achieved results suggest that both electrical parameters of the generator (PV and PRF) affect the plasma UV component. However, for the operating conditions considered in this paper, the values obtained for the UV irradiance are compatible with biomedical applications.

Axial temperature profiles confirm that the plasma source driven by nanosecond pulses can generate a plasma jet with temperature compatible with heat-sensitive materials, including biological substrates.

The presented results provide some fundamental understanding of the characteristics and behavior of the discharge generated by an APPJ driven by nanosecond voltage pulses; this can support the development of a wide range of applications such as surface functionalization, thin film deposition, electrospinning of polymers, and nanoadditive dispersion in polymer solutions.

REFERENCES

[1] K. D. Weltmann *et al.*, "Antimicrobial treatment of heat sensitive products by miniaturized atmospheric pressure plasma jets (APPJs)," *J. Phys. D, Appl. Phys.*, vol. 41, no. 19, pp. 194008–194014, Sep. 2008.

[2] J. Shen *et al.*, "Sterilization of *Bacillus subtilis* spores using an atmospheric plasma jet with argon and oxygen mixture gas," *Appl. Phys. Exp.*, vol. 5, no. 3, p. 036201, Feb. 2012.

[3] U. Lommatzsch, D. Pasedag, A. Baalmann, G. Ellinghorst, and H.-E. Wagner, "Atmospheric pressure plasma jet treatment of polyethylene surfaces for adhesion improvement," *Plasma Process. Polym.*, vol. 4, no. 1 pp. S1041–S1045, Apr. 2007.

[4] C. Cheng, Z. Liye, and R.-J. Zhan, "Surface modification of polymer fibre by the new atmospheric pressure cold plasma jet," *Surf. Coat. Technol.*, vol. 200, no. 24, pp. 6659–6665, Aug. 2006.

[5] E. J. Szili, S. A. Al-Bataineh, P. M. Bryant, R. D. Short, J. W. Bradley, and D. A. Steele, "Controlling the spatial distribution of polymer surface treatment using atmospheric-pressure microplasma jets," *Plasma Process. Polym.*, vol. 8, no. 1, pp. 38–50, Jan. 2011.

[6] X. Deng *et al.*, "Engineering of composite organosilicon thin films with embedded silver nanoparticles via atmospheric pressure plasma process for antibacterial activity," *Plasma Process. Polym.*, vol. 11, no. 10, pp. 921–930, 2014.

[7] H. Fakhouri, D. B. Salem, O. Carton, J. Pulpytel, and F. Arefi-Khonsari, "Highly efficient photocatalytic TiO_2 coatings deposited by open air atmospheric pressure plasma jet with aerosolized TTIP precursor," *J. Phys. D, Appl. Phys.*, vol. 47, no. 26, pp. 265301–265312, Jun. 2014.

[8] D. Mariotti and M. Sankaran, "Perspectives on atmospheric-pressure plasmas for nanofabrication," *J. Phys. D, Appl. Phys.*, vol. 44, no. 17, pp. 174023–174031, Apr. 2011.

[9] D. Mariotti, J. Patel, V. Svrcek, and P. Maguire, "Plasma–liquid interactions at atmospheric pressure for nanomaterials synthesis and surface engineering," *Plasma Process. Polym.*, vol. 9, nos. 11–12, pp. 1074–1085, Dec. 2012.

[10] S. Mitra, V. Svrcek, D. Mariotti, T. Velusamy, K. Matsubara, and M. Kondo, "Microplasma-induce liquid chemistry for stabilizing of silicon nanocrystals optical properties in water," *Plasma Process. Polym.*, vol. 11, no. 2, pp. 158–163, Feb. 2014.

[11] S. W. Lee, D. Liang, X. P. A. Gao, and R. M. Sankaran, "Direct writing of metal nanoparticles by localized plasma electrochemical reduction of metal cations in polymer films," *Adv. Funct. Mater.*, vol. 21, no. 11, pp. 2155–2161, Jun. 2011.

[12] S. W. Lee, C. Mattevi, M. Chhowalla, and R. M. Sankaran, "Plasma-assisted reduction of graphene oxide at low temperature and atmospheric pressure for flexible conductor applications," *J. Phys. Chem. Lett.*, vol. 3, no. 6, pp. 772–777, Feb. 2012.

[13] I. E. Kieft, M. Kurdi, and E. Stoffels, "Reattachment and apoptosis after plasma-needle treatment of cultured cells," *IEEE Trans. Plasma Sci.*, vol. 34, no. 4, pp. 1331–1336, Aug. 2006.

[14] G. Fridman *et al.*, "Blood coagulation and living tissue sterilization by floating-electrode dielectric barrier discharge in air," *Plasma Chem. Plasma Process.*, vol. 26, no. 4, pp. 425–442, Aug. 2006.

[15] G. Fridman, G. Friedman, A. Gutsol, A. B. Shekhter, V. N. Vasilets, and A. Fridman, "Applied plasma medicine," *Plasma Process. Polym.*, vol. 5, no. 6, pp. 503–533, Aug. 2008.

[16] G.-C. Kim, H. J. Lee, and C.-H. Shon, "The effects of a micro plasma on melanoma (G361) cancer cells," *J. Korean Phys. Soc.*, vol. 54, no. 2, pp. 628–632, 2009.

[17] C.-H. Kim *et al.*, "Induction of cell growth arrest by atmospheric non-thermal plasma in colorectal cancer cells," *J. Biotechnol.*, vol. 150, no. 4, pp. 530–538, Dec. 2010.

[18] M. Keidar *et al.*, "Cold plasma selectivity and the possibility of a paradigm shift in cancer therapy," *Brit. J. Cancer*, vol. 105, no. 9, pp. 1295–1301, 2011.

[19] H. Kurita *et al.*, "Single-molecule measurement of strand breaks on large DNA induced by atmospheric pressure plasma jet," *Appl. Phys. Lett.*, vol. 99, no. 19, p. 191504, 2011.

[20] X. Yan *et al.*, "Plasma-induced death of HepG2 cancer cells: Intracellular effects of reactive species," *Plasma Process. Polym.*, vol. 9, no. 1, pp. 59–66, Jan. 2012.

[21] J. Huang *et al.*, "Dielectric barrier discharge plasma in Ar/O_2 promoting apoptosis behavior in A549 cancer cells," *Appl. Phys. Lett.*, vol. 99, no. 25, p. 253701, 2011.

[22] H. M. Joh, S. J. Kim, T. H. Chung, and S. H. Leem, "Reactive oxygen species-related plasma effects on the apoptosis of human bladder cancer cells in atmospheric pressure pulsed plasma jets," *Appl. Phys. Lett.*, vol. 101, no. 5, p. 053703, 2012.

[23] O. Volotskova, T. S. Hawley, M. A. Stepp, and M. Keidar, "Targeting the cancer cell cycle by cold atmospheric plasma," *Sci. Rep.*, vol. 2, no. 636, pp. 636–645, Sep. 2012.

[24] J. F. Kolb, A. M. Mattson, C. M. Edelblute, X. Hao, M. A. Malik, and L. C. Heller, "Cold DC-operated air plasma jet for the inactivation of infectious microorganisms," *IEEE Trans. Plasma Sci.*, vol. 40, no. 11, pp. 3007–3026, Nov. 2012.

[25] R. Jijie, C. Luca, V. Pohoata, and I. Topala, "Effects of atmospheric-pressure plasma jet on pepsin structure and function," *IEEE Trans. Plasma Sci.*, vol. 40, no. 11, pp. 2980–2985, Nov. 2012.

[26] S. Zhao *et al.*, "Combined effect of N-acetylcysteine (NAC) and plasma on proliferation of HepG2 cells," *IEEE Trans. Plasma Sci.*, vol. 40, no. 9, pp. 2179–2184, Sep. 2012.

[27] L. Brulle *et al.*, "Effects of a non thermal plasma treatment alone or in combination with gemcitabine in a MIA PaCa2-luc orthotopic pancreatic carcinoma model," *PLoS ONE*, vol. 7, p. e52653, Dec. 2012.

[28] X. Lu, M. Laroussi, and V. Puech, "On atmospheric-pressure non-equilibrium plasma jets and plasma bullets," *Plasma Sour. Sci. Technol.*, vol. 21, no. 3, p. 034005, Apr. 2012.

[29] E. Stoffels, A. J. Flikweert, W. W. Stoffels, and G. M. W. Kroesen, "Plasma needle: A non-destructive atmospheric plasma source for fine surface treatment of (bio)materials," *Plasma Sour. Sci. Technol.*, vol. 11, no. 4, pp. 383–388, Aug. 2002.

[30] E. Robert *et al.*, "Experimental study of a compact nanosecond plasma gun," *Plasma Process. Polym.*, vol. 6, no. 12, pp. 795–802, Dec. 2009.

[31] M. Laroussi and X. Lu, "Room-temperature atmospheric pressure plasma plume for biomedical applications," *Appl. Phys. Lett.*, vol. 87, no. 11, p. 113902, 2005.

[32] K.-D. Weltmann *et al.*, "Atmospheric pressure plasma jet for medical therapy: Plasma parameters and risk estimation," *Contrib. Plasma Phys.*, vol. 49, no. 9, pp. 631–640, Nov. 2009.

[33] J. Y. Kim, J. Ballato, and S.-O. Kim, "Intense and energetic atmospheric pressure plasma jet arrays," *Plasma Process. Polym.*, vol. 9, no. 3, pp. 253–260, Mar. 2012.

[34] S. Bianconi *et al.*, "iCCD imaging of the transition from uncoupled to coupled mode in a plasma source for biomedical and materials treatment applications," *IEEE Trans. Plasma Sci.*, vol. 42, no. 10, pp. 2746–2747, Oct. 2014.

[35] K. Kim, G. Kim, Y. C. Hong, and S. S. Yang, "A cold micro plasma jet device suitable for bio-medical applications," *Microelectron. Eng.*, vol. 87, nos. 5–8, pp. 1177–1180, May/Aug. 2010.

[36] F. T. O'Neill *et al.*, "Generation of active species in a large atmospheric-pressure plasma jet," *IEEE Trans. Plasma Sci.*, vol. 40, no. 11, pp. 2994–3002, Nov. 2012.

[37] X. L. Deng, A. Y. Nikiforov, P. Vanraes, and C. Leys, "Direct current plasma jet at atmospheric pressure operating in nitrogen and air," *J. Appl. Phys.*, vol. 13, no. 2, p. 023305, 2013.

[38] Q. Xiong *et al.*, "Absolute OH density determination by laser induced fluorescence spectroscopy in an atmospheric pressure RF plasma jet," *Eur. Phys. J. D*, vol. 66, p. 281, Nov. 2012.

[39] Y. Hong, N. Lu, J. Pan, J. Li, Y. Wu, and K. F. Shang, "Characteristic study of cold atmospheric argon plasma jets with rod-tube/tube high voltage electrode," *J. Electrostatics*, vol. 71, no. 2, pp. 93–111, Apr. 2013.

[40] A. F. H. van Gessel, B. Hrycak, M. Jasinski, J. Mizeraczyk, J. J. A. M. van der Mullen, and P. J. Bruggeman, "Temperature and NO density measurements by LIF and OES on an atmospheric pressure plasma jet," *J. Phys. D, Appl. Phys.*, vol. 46, no. 9, p. 095201, 2013.

[41] Q. Xiong, A. Y. Nikiforov, M. A. Gonzalez, C. Leys, and X. P. Lu, "Characterization of an atmospheric helium plasma jet by relative and absolute optical emission spectroscopy," *Plasma Sour. Sci. Technol.*, vol. 22, no. 1, p. 015011, Dec. 2013.

[42] E. Karakas and M. Laroussi, "Experimental studies on the plasma bullet propagation and its inhibition," *J. Appl. Phys.*, vol. 108, no. 6, p. 063305, 2012.

[43] M. Teschke, J. Kedzierski, E. G. Finantu-Dinu, D. Korzec, and J. Engemann, "High-speed photographs of a dielectric barrier atmospheric pressure plasma jet," *IEEE Trans. Plasma Sci.*, vol. 33, no. 2, pp. 310–311, Apr. 2005.

[44] X. Lu and M. Laroussi, "Dynamics of an atmospheric pressure plasma plume generated by submicrosecond voltage pulses," *J. Appl. Phys.*, vol. 100, no. 6, p. 063302, 2006.

[45] C. Cachoncinlle, R. Viladrosa, E. Robert, J.-M. Pouvesle, A. Khacef, and S. Dozias, "Transient plasma ball generation system at long distance," U.S. Patent 8 482 206 B2, Jul. 9, 2013.

[46] E. Robert, V. Sarron, D. Ries, S. Dozias, M. Vandamme, and J. M. Pouvesle, "Characterization of pulsed atmospheric-pressure plasma streams (PAPS) generated by a plasma gun," *Plasma Sour. Sci. Technol.*, vol. 21, no. 3, p. 034017, May 2012.

[47] Z. Xiong, E. Robert, V. Sarron, J.-M. Pouvesle, and M. J. Kushner, "Dynamics of ionization wave splitting and merging of atmospheric-pressure plasmas in branched dielectric tubes and channels," *J. Phys. D, Appl. Phys.*, vol. 45, no. 7, pp. 275201–275220, Jun. 2012.

[48] X. Lu, G. V. Naidis, M. Laroussi, and K. Ostrikov, "Guided ionization waves: Theory and experiments," *Phys. Rep.*, vol. 540, no. 3, pp. 123–166, Jul. 2014.

[49] D. Fabiani *et al.*, "Plasma assisted nanoparticle dispersion in polymeric solutions for the production of electrospun lithium battery separators," in *Proc. IEEE Int. Conf. Solid Dielectr. (ICSD)*, Bologna, Italy, Jun./Jul. 2013, pp. 718–721.

[50] V. Colombo *et al.*, "Atmospheric pressure non-equilibrium plasma treatment to improve the electrospinnability of poly(L-lactic acid) polymeric solution," *Plasma Process. Polym.*, vol. 11, no. 3, pp. 247–255, Mar. 2014.

[51] D. Fabiani *et al.*, "Study of the effect of atmospheric pressure plasma treatment on electrospinnability of poly-L-lactic acid solutions: Voltage waveform effect," in *Proc. IEEE Int. Conf. Solid Dielectr. (ICSD)*, Bologna, Italy, Jun./Jul. 2013, pp. 358–361.

[52] M. Boselli *et al.*, "Schlieren high-speed imaging of a nanosecond pulsed atmospheric pressure non-equilibrium plasma jet," *Plasma Chem. Plasma Process.*, vol. 34, no. 4, pp. 853–869, Jul. 2014.

[53] M. R. Wertheimer, B. Saoud, M. Ahlawat, and R. Kashyap, "Accurate in-situ gas temperature measurements in dielectric barrier discharges at atmospheric pressure," *J. Appl. Phys*, vol. 100, no. 20, p. 201112, 2012.

[54] A. Shashurin, M. N. Shneider, and M. Keidar, "Measurements of streamer head potential and conductivity of streamer column in cold non-equilibrium atmospheric plasmas," *Plasma Sour. Sci. Technol.*, vol. 21, no. 3, p. 034006, 2012.

[55] Y. Xian *et al.*, "From short pulses to short breaks: Exotic plasma bullets via residual electron control," *Sci. Rep.*, vol. 3, Apr. 2013, Art. ID 1599.

[56] C. Jiang, M. T. Chen, and M. A. Gundersen, "Polarity-induced asymmetric effects of nanosecond pulsed plasma jets," *J. Phys. D, Appl. Phys.*, vol. 42, no. 23, p. 232002, Nov. 2009.

[57] J. P. Boeuf, L. L. Yang, and L. C. Pitchford, "Dynamics of a guided streamer ('plasma bullet') in a helium jet in air at atmospheric pressure," *J. Phys. D, Appl. Phys.*, vol. 46, no. 1, pp. 015201–0152014, 2013.
[58] S. Wu, H. Xu, X. Lu, and Y. Pan, "Effect of pulse rising time of pulse dc voltage on atmospheric pressure non-equilibrium plasma," *Plasma Process. Polym.*, vol. 10, no. 2, pp. 136–140, Feb. 2013.
[59] S. Wu, Z. Wang, Q. Huang, X. Tan, X. Lu, and K. Ostrikov, "Atmospheric-pressure plasma jets: Effect of gas flow, active species, and snake-like bullet propagation," *Phys. Plasmas*, vol. 20, no. 2, p. 023503, Feb. 2013.
[60] R. Xiong, Q. Xiong, A. Y. Nikiforov, P. Vanraes, and C. Leys, "Influence of helium mole fraction distribution on the properties of cold atmospheric pressure helium plasma jets," *J. Appl. Phys.*, vol. 112, no. 3, p. 033305, 2012.
[61] N. Y. Babaeva and M. J. Kushner, "Interaction of multiple atmospheric-pressure micro-plasma jets in small arrays: He/O_2 into humid air," *Plasma Sour. Sci. Technol.*, vol. 23, no. 1, p. 015007, Jan. 2014.
[62] Y. Sakiyama and D. B. Graves, "Neutral gas flow and ring-shaped emission profile in non-thermal RF-excited plasma needle discharge at atmospheric pressure," *Plasma Sour. Sci. Technol.*, vol. 18, no. 2, p. 025022, Mar. 2009.
[63] D. Dobrynin, K. Arjunan, A. Fridman, G. Friedman, and A. M. Clyne, "Direct and controllable nitric oxide delivery into biological media and living cells by a pin-to-hole spark discharge (PHD) plasma," *J. Phys. D, Appl. Phys.*, vol. 44, no. 7, p. 075201, Jan. 2011.
[64] T. G. Klampfl *et al.*, "Cold atmospheric air plasma sterilization against spores and other microorganisms of clinical interest," *Appl. Environ. Microbiol.*, vol. 78, no. 15, pp. 5077–5082, May 2012.
[65] T. Shimizu *et al.*, "Characterization of microwave plasma torch for decontamination," *Plasma Process. Polym.*, vol. 5, no. 6, pp. 577–582, Aug. 2008.

Marco Boselli was born in Italy in 1983. He received the master's degree in energy engineering from the Alma Mater Studiorum-Università di Bologna, Bologna, Italy, in 2009, with a focus on industrial applications of thermal plasmas.

He has been a Researcher in modeling and diagnostics on metal cutting and welding plasma processes with the Interdepartmental Center for Industrial Research-Advanced Applications in Mechanical Engineering and Materials Technology, Alma Mater Studiorum-Università di Bologna, since 2011.

Vittorio Colombo was born in Italy in 1961. He received the master's degree in nuclear engineering and the Ph.D. degree in energetics from the Politecnico di Turin, Turin, Italy, in 1986 and 1990, respectively.

He was with the Nuclear Reactor Physics Group, Politecnico di Turin, as a Researcher, from 1990 to 1992. Since 1992, he has been with the Faculty of Engineering, Alma Mater Studiorum-Università di Bologna, Bologna, Italy, where he has been a Full Professor of Industrial Applications of Plasmas with the Department of Industrial Engineering since 2000. Since 2010, he has been a member of the Interdepartmental Center for Industrial Research-Advanced Applications in Mechanical Engineering and Materials Technology with the Alma Mater Studiorum-Università di Bologna.

Matteo Gherardi was born in Italy in 1985. He received the master's degree in energy engineering from the Alma Mater Studiorum-Università di Bologna, Bologna, Italy, in 2009, and the Ph.D. degree in industrial applications of plasmas from the Department of Industrial Engineering, Alma Mater Studiorum-Università di Bologna, in 2013.

He has been a Post-Doctoral Researcher with the Alma Mater Studiorum-Università di Bologna since 2013. His current research interests include plasma assisted nanoparticle synthesis and plasma biomedical applications.

Romolo Laurita was born in Italy in 1986. He received the master's degree in energy engineering from the Alma Mater Studiorum-Università di Bologna, Bologna, Italy, in 2011, where he is currently pursuing the Ph.D. degree in industrial applications of plasmas.

His current research interests include design and characterization of atmospheric pressure nonthermal plasma sources for biomedical applications.

Anna Liguori was born in Italy in 1989. She received the master's degree in energy engineering from the Alma Mater Studiorum-Università di Bologna, Bologna, Italy, in 2012, where she is currently pursuing the Ph.D. degree in industrial applications of plasmas. Her master's degree thesis was on characterization of atmospheric cold plasma sources for scaffold biocompatibilzation.

Paolo Sanibondi was born in Italy in 1983. He received the master's degree in energy engineering from the Alma Mater Studiorum-Università di Bologna, Bologna, Italy, in 2007, and the Ph.D. degree in industrial applications of thermal plasmas from the Department of Mechanical Engineering, Alma Mater Studiorum-Università di Bologna, in 2011.

He has been a Post-Doctoral Researcher with the Alma Mater Studiorum-Università di Bologna, since 2011, where he is involved in plasma modeling and diagnostics.

Emanuele Simoncelli was born in Italy in 1990. He received the master's degree in energy engineering from the Alma Mater Studiorum-Università di Bologna, Bologna, Italy, in 2014, where he is currently pursuing the Ph.D. degree in industrial applications of plasmas.

Augusto Stancampiano was born in Italy in 1987. He received the master's degree in energy engineering from the Alma Mater Studiorum-Università di Bologna, Bologna, Italy, in 2012, where he is currently pursuing the Ph.D. degree in industrial applications of plasmas. His master's degree thesis was on the characterization of atmospheric cold plasma sources and their possible applications in the functionalization of polylactic acid films.